High Integrity Stochastic Modeling of GPS Receiver Clock for Improved Positioning and Fault Detection Performance

Fang-Cheng Chan, Mathieu Joerger and Boris Pervan
Navigation and Guidance Laboratory, Department of Mechanical Material and Aerospace Engineering
Illinois Institute of Technology
Chicago, IL, US
chanfan@iit.edu

***Abstract*—In this paper, a validated stochastic clock random error model is used to derive a correct time correlation matrix for a sequence of clock random errors. A batch estimator incorporating the complete time correlation matrix is developed to account for clock random errors. Performance improvement for the proposed receiver clock-aided navigation system is fully investigated. A benchmark application of an aircraft precision approach is used to evaluate the system availability performance with a single satellite failure assumption.**

Keywords—GPS; stochastic clock error model; receiver clock aiding; high integrity navigation

I. INTRODUCTION

Receiver clock aiding has great potential to improve GPS-based navigation systems in vertical position accuracy, integrity, continuity and availability. A perfect receiver clock is equivalent to adding one extra perfect measurement (clock measurement), which strongly influences vertical position estimation. Therefore, better vertical position accuracy and fault detection performance (provided by increased measurement redundancy) can be expected from a perfect receiver clock-aided GPS navigation system. With current technologies, a high quality (albeit, not perfect) receiver clock is feasible and affordable to many GPS navigation system users. A receiver clock-aided GPS navigation system is well suited to integrity-driven applications (for example, aviation). The key point in this paper is to protect the integrity of the receiver clock aided system by ensuring the integrity of the clock model itself.

Traditionally, receiver clock aiding is done either through a least squares process that fits a series of clock estimates to a linear model [1] or through a Kalman filter which utilizes a clock dynamic model with non-time-correlated process noise [2]. Basically, they are all based on a fundamental clock error model:

$$\Delta\theta_k = \Delta\theta_0 + \Delta f_0 \times k \times \Delta t + \delta\theta_k \qquad (1)$$

where $\Delta\theta_k$ is the clock phase deviation at epoch k, $\Delta\theta_0$ and Δf_0 are the initial clock phase and frequency deviations respectively, Δt is the sampling period, and $\delta\theta_k$ is the clock phase random coasting error at epoch k.

Existing methods in [1] and [2] implement simplified clock random error models whose effect on system integrity is unknown. To ensure clock-aided navigation system integrity, a clock-phase error model providing a statistical description of the random clock error over time is needed. Stochastic models for clock-phase random coasting error have been developed in the past in [2] and [3]. However, implementation of a clock stochastic model in GPS positioning has not been addressed.

A stochastic model for clock-phase random coasting error was re-visited and validated for high-quality atomic clocks in [4]. In this paper, the complete time correlation of clock random errors is analytically derived using the clock error model validated in [4]. A batch estimator that correctly accounts for the time correlation of receiver clock random errors is developed to ensure the integrity of position estimation of a clock-aided navigation system. In addition, a more traditional two-state Kalman filter model for receiver clock aiding is compared with new batch estimator to illustrate the fundamental difference in handling clock-phase coasting errors in time. The batch estimator is shown to account for the clock random error more rigorously than the traditional Kalman filter implementation.

The positioning performance of the batch estimator without receiver clock aiding is also investigated. An equivalency in position accuracy between batch position estimation and snap-shot positioning is analytically derived. When the natural satellite geometry variations are taken into account in the batch interval, significant improvement in position accuracy can be achieved for the batch estimator. The improvement results from enhanced observability on carrier-phase ambiguities provided by geometry change. It is also shown that accuracy improvement with receiver clock aiding is minimal, but that the main advantage of receiver clock aiding is improving the system integrity.

A solution separation detection scheme using a multiple-hypothesis approach is adopted as the means for fault detection [5] [6]. Reduction in vertical protection level (VPL) is quantified by comparing VPLs generated for a traditional smoothed code positioning process and for the batch estimator with and without receiver clock aiding. It is shown that a high-quality receiver clock can significantly improve both the system availability and continuity.

In the end, aircraft precision approach navigation is selected as benchmark application to evaluate the system performance for the high-integrity receiver clock-aided batch estimator. It is implemented in the context of the GNSS Evolutionary Architecture Study (GEAS), an FAA effort to define and evaluate potential navigation architectures for global aircraft precision approach capability (LPV-200 [8]). A candidate GEAS architecture, which is called Advanced RAIM (receiver autonomous integrity monitoring) or ARAIM [5] [7], is adopted. In the frame work of the GEAS ARAIM architecture, we analyze the availability achievable for the batch estimator navigation system with various clock-aiding scenarios. The performance results for the receiver clock aided systems are very encouraging in terms of the global coverage of achieving 99.5% availability.

II. Stochastic Clock Error Model and Time Correlation of Clock Random Errors

A. Stochastic Clock Error Model

As shown in equation (1), the clock phase deviation of a stable clock can be generally modeled as the sum of an initial phase offset, the time-linear phase deviation from an initial frequency offset and a clock-phase random coasting error. The clock-phase random coasting error is caused by clock frequency instability. The randomness of frequency errors results in unpredictable clock-phase random errors. Therefore, a stochastic model is needed to mathematically describe the dynamics of clock-phase coasting errors.

A previously validated stochastic clock error model has been developed in [2] [3]. The model is derived from three frequency error sources: white frequency error, flicker frequency error and random walk frequency error. The corresponding power spectrum for the three frequency errors is:

$$S_f(f) = h_0 f^0 + h_{-1} f^{-1} + h_{-2} f^{-2} \tag{2}$$

where h_0 is the magnitude of the frequency power for white frequency error, h_{-1} and h_{-2} are the magnitudes of the frequency power for flicker and random walk frequency errors respectively, and f is Fourier frequency in Hz.

The variance of the stochastic clock-phase error resulting from (2) is derived in [2], [3] and [4] as:

$$\sigma_{\delta\theta}^2(\Delta t) = \frac{h_0}{2}\Delta t + 2h_{-1}\Delta t^2 + \frac{2\pi^2}{3}h_{-2}\Delta t^3 \tag{3}$$

where $\sigma_{\delta\theta}^2$ is the variance of the clock-phase random coasting error and Δt is the coasting time. Table I lists example frequency power spectrum magnitudes for different clock qualities.

The clock model validity and the period over which (3) is applicable (up to 60 minutes for the clocks in Table I) have been studied in [4].

TABLE I. QUALITY OF DIFFERENT CLOCKS

Clock Type	Frequency Power Spectrum Coefficient		
	h_0	h_{-1}	h_{-2}
Chip-scale atomic clock [9]	8×10^{-21}	2.9×10^{-22}	6.1×10^{-25}
Rubidium clock [10]	5.3×10^{-22}	0	1.2×10^{-31}
Cesium clock [10]	1.1×10^{-22}	2.1×10^{-28}	0

B. Time Correlaton of Clock Random Errors

Clock-phase random coasting errors result from the integration of frequency errors over time. Hence, they are correlated in time. The time correlation of clock random phase errors has to be accounted for to ensure the integrity of a GPS navigation system using receiver clock aiding. An equation for the time correlation of clock random phase errors has been previously derived in [3]. We revisit the derivation in Appendix A. To derive the time correlation of clock random errors, the same methodology used to compute (3) is employed. The result for time correlation between clock-phase random errors at coasting times Δt_i and Δt_j is shown below:

$$R_{\delta\theta}(\Delta t_i, \Delta t_j) = \begin{cases} \dfrac{h_0}{2}\Delta t_i + 2h_{-1}\Delta t_i^{\,2} + \dfrac{2\pi^2}{3}h_{-2}\Delta t_i^{\,3}, i = j \\ R_{\delta\theta_0}(\Delta t_i, \Delta t_j) + R_{\delta\theta_{-1}}(\Delta t_i, \Delta t_j) \\ + R_{\delta\theta_{-2}}(\Delta t_i, \Delta t_j), i < j \end{cases} \tag{4}$$

where $R_{\delta\theta_0}$, $R_{\delta\theta_{-1}}$ and $R_{\delta\theta_{-2}}$ are:

$$R_{\delta\theta_0}(\Delta t_i, \Delta t_j) = \frac{h_0}{2}\Delta t_i$$

$$R_{\delta\theta_{-1}}(\Delta t_i, \Delta t_j) = h_{-1}[(\Delta t_i + \Delta t_j)\sqrt{\Delta t_i \Delta t_j} - (\Delta t_j - \Delta t_i)^2 \ln\left|\frac{\sqrt{\Delta t_i} + \sqrt{\Delta t_j}}{\sqrt{(\Delta t_j - \Delta t_i)}}\right|]$$

$$R_{\delta\theta_{-2}}(\Delta t_i, \Delta t_j) = 2\pi^2 h_{-2}[\frac{\Delta t_i^3}{3} + \frac{\Delta t_i^2}{2}(\Delta t_j - \Delta t_i)]$$

Considering a sequence of clock measurements described in (1), the sequence of clock random coasting error components can be arranged in vector from:

$$\vec{s}_w = \left[\delta\theta(\Delta t_1) \quad \delta\theta(\Delta t_2) \quad \cdots \quad \delta\theta(\Delta t_k)\right]^T$$

Then, a complete time correlation matrix for the clock random error sequence can be obtained by:

$$W_{\delta\theta}(\Delta t_1 \to \Delta t_k) = E\left[\vec{s}_w \vec{s}_w{}^T\right] = \begin{bmatrix} R_{\delta\theta}(\Delta t_1, \Delta t_1) & R_{\delta\theta}(\Delta t_1, \Delta t_2) & \cdots & R_{\delta\theta}(\Delta t_1, \Delta t_k) \\ R_{\delta\theta}(\Delta t_2, \Delta t_1) & R_{\delta\theta}(\Delta t_2, \Delta t_2) & & \vdots \\ \vdots & & \ddots & \vdots \\ R_{\delta\theta}(\Delta t_k, \Delta t_1) & \cdots & \cdots & R_{\delta\theta}(\Delta t_k, \Delta t_k) \end{bmatrix} \quad (5)$$

where $W_{\delta\theta}$ is the time correlation matrix for clock random errors.

The diagonal elements in the time correlation matrix are the variances of clock random errors shown in (3). The off diagonal terms are obtained by using the time correlation equation (4) to complete the time correlation matrix for clock random errors.

III. Optimal Batch Estimator for Receiver Clock-Aided Position Estimation

To exploit the time correlation information derived from the clock random error model, a batch-type estimator is selected for its ability to accommodate the complete clock time correlation matrix. This batch estimator is implemented as a moving window with a fixed batch interval. A 30 minute batch interval is chosen, which ensures validity of the clock error model and limits the computational burden. Smoothed codes and carrier measurements in the batch interval are sampled at two times the smoothing time (at which time-epochs measurements are assumed independent), and the correlation between smoothed code and carrier measurements is modeled.

The proposed receiver clock-aided batch estimator is compared to a traditional Kalman filter using a two-state clock model [2]. To clarify the comparison, the Kalman filter implementation is converted into an equivalent batch estimator. Both estimators are assuming the same simple measurement model of a direct measurement on the clock phase with white measurement noise. The details of Kalman-to-batch conversion is shown in Appendix B. The resulting measurement covariance matrices for these two batch estimators are shown below:

$$\mathrm{cov}(\vec{v}_{BE}) = \begin{bmatrix} \mathrm{cov}(v) & 0 & 0 \\ 0 & P_0 & 0 \\ 0 & 0 & W_{\delta\theta}(\Delta t \to k\Delta t) \end{bmatrix} \quad (6)$$

$$\mathrm{cov}(\vec{v}_{KF}) = \begin{bmatrix} \mathrm{cov}(v) & 0 & 0 \\ 0 & P_0 & 0 \\ 0 & 0 & W_{\delta\theta,\delta f}(\Delta t \to k\Delta t) \end{bmatrix} \quad (7)$$

where cov(v) is the clock-phase measurement white noise covariance and P_0 is the prior knowledge on initial clock phase and frequency offsets. $W_{\delta\theta}(\Delta t \to k\Delta t)$ and $W_{\delta\theta,\delta f}(\Delta t \to k\Delta t)$ are the uncertainties covariance on clock pseudo-measurements:

$$W_{\delta\theta}(\Delta t \to k\Delta t) = \begin{bmatrix} R_{\delta\theta}(\Delta t, \Delta t) & R_{\delta\theta}(\Delta t, 2\Delta t) & \cdots & R_{\delta\theta}(\Delta t, k\Delta t) \\ R_{\delta\theta}(2\Delta t, \Delta t) & R_{\delta\theta}(2\Delta t, 2\Delta t) & & \vdots \\ \vdots & & \ddots & \vdots \\ R_{\delta\theta}(k\Delta t, \Delta t) & \cdots & \cdots & R_{\delta\theta}(k\Delta t, k\Delta t) \end{bmatrix} \quad (8)$$

$$W_{\delta\theta,\delta f}(\Delta t \to k\Delta t) = \begin{bmatrix} W_{\delta\theta,\delta f}(\Delta t) & 0 & \cdots & 0 \\ 0 & W_{\delta\theta,\delta f}(\Delta t) & & \vdots \\ \vdots & & \ddots & \vdots \\ 0 & \cdots & \cdots & W_{\delta\theta,\delta f}(\Delta t) \end{bmatrix} \quad (9)$$

The measurement covariance matrices, as shown in (6) and (7), for both estimators are made of the white noise measurement covariance, the prior knowledge on initial clock phase and frequency offsets, and the time correlation matrix for clock random errors. The first two block diagonal matrices are identical for both estimators. However, the optimal batch estimator utilizes the complete time correlation matrix (including off-diagonal terms), as shown in (8), to account for clock random errors. The Kalman-filter-equivalent batch estimator uses a sequence of diagonal matrix blocks for clock errors as shown in (9) that are mutually uncorrelated. The model used in the batch estimator contains all correlation information and is therefore mathematically rigorous.

IV. Positioning Accuracy Improvement

A. Relationship between Batch Position Estimation and Snap-shot Positioing

Positioning performance of the batch estimator itself has to be investigated first before studying the benefit of receiver clock aiding. In this section, the relation between the batch position estimation using code and carrier measurements and snap-shot positioning using smoothed code is established. The same measurements are used (code and carrier measurements) but the two processes yield different results.

For clarity of explanation, code and carrier multipath errors are considered as the only error source. Vertical position estimation over one day at one location are computed using the batch estimator without clock aiding. A '27 minus one' constellation [7] is adopted and the 30 minute batch interval is used. 100 second-smoothed code and raw carrier measurements are sampled at 200 second intervals. The resulting measurement errors are therefore assumed uncorrelated in the batch interval. The correlation between the smoothed code and carrier is analyzed in Appendix C. Satellite geometries are intentionally kept unchanged within the batch interval (no SV motion). Vertical position standard deviations over 24 hours are shown in Fig. 1. The performance of two snap-shot

positioning examples using smoothed codes is displayed in Fig.1 as well. The red curve is the 1000-second smoothed code positioning performance, and the blue curve is using 30 minute smoothing time. The 1000 second smoothing time was derived analytically as being equivalent to the batch estimator assuming that raw code and carrier multipath errors are uncorrelated in time (β_1=0 and β_2=0 in Appendix C). The derivation of the smoothed code standard deviation with various smoothing times is detailed in Appendix C.

The curves in Fig. 1 for the batch position estimation and 1000-second smoothed code positioning are overlapping. This outcome matches the analytical derivation. It proves that the performance of batch position estimation with frozen SV geometry is equivalent to that of smoothed code positioning. The performance for 30 minute-smoothed code positioning is the best among three due to longer smoothing time.

The same simulation for the batch estimator is now performed again, but without freezing the geometry. The results are shown in Fig. 2, in which the batch estimator clearly outperforms the other processes. The results in Fig. 2 demonstrate the benefit of geometry change for a batch estimation using code and carrier measurements. The reason for superior batch estimation performance is that the geometry change provides better observability on floating carrier ambiguities.

B. Accuracy Improvement for Reciver Clock Aiding

The positioning accuracy improvement of receiver clock aiding is studied by comparing the positioning accuracy of batch estimator with and without clock aiding. The aforementioned scenario (27 minus one constellation, multipath error only) is simulated for the batch estimator with rubidium clock aiding (which quality is listed in Table I). The resulting vertical position standard deviation differs very slightly from that of the batch estimator without clock aiding. The third curve in Fig. 3 represents the performance of a system using a virtual clock model which has 100-times better quality than the cesium atomic clock in Table I. No obvious deviation can be observed either. Therefore, we can conclude that the positioning accuracy improvement for receiver clock-aided

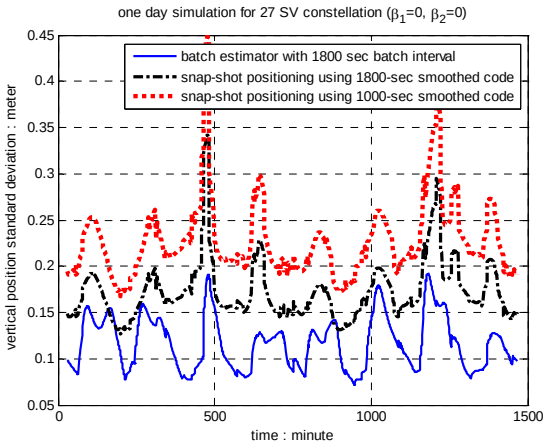

Figure 2. Benefit of satellite geometry change for batch estimation

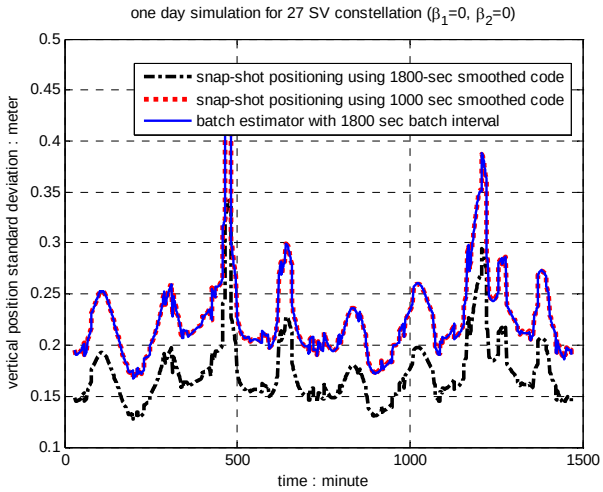

Figure 1. Performance of batch estimator and smoothed code positioning

batch position estimation is negligible. The same result was observed for other simulated satellite geometries.

However, the main advantage of using receiver clock aiding is to improve the system integrity, especially when the satellite geometry is poor. The integrity improvement is provided by added system redundancy from the receiver clock model. This statement is demonstrated in following sections.

V. FAULT DETECTION PERFORMANCE AND SYSTEM INTEGRITY IMPROVEMENT USING HIGH-INTERITY RECEIVER CLOCK AIDING

Methods to compute the system integrity are briefly introduced first. The well-known solution separation fault detection algorithm using the multiple hypothesis approach is adopted as the means to secure the system integrity under a measurement fault condition [5] [6]. A flexible integrity risk allocation algorithm was implemented for batch estimator fault detection as well [6]. Because measurements at multiple time epochs are included in one batch estimation, a prior probability of at least one measurement fault for single satellite failure has to be derived. An independent satellite failure rate of $1x10^{-5}$/hr /sv and mean one hour delay for the GPS control segment to

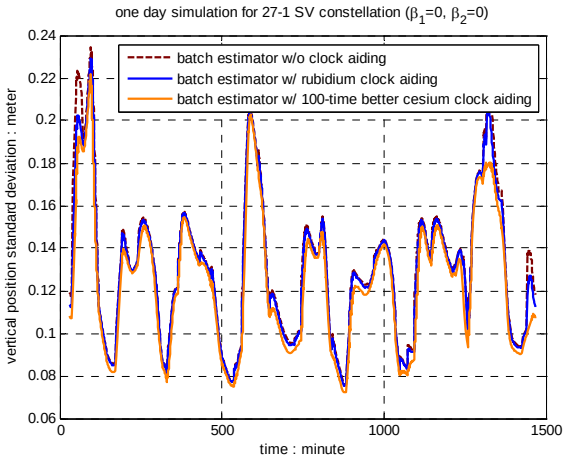

Figure 3. Performance of batch estimator with and without receiver clock aiding

inform users are assumed [5]. A conservative result is shown below. The details can be found in Appendix D.

$$P_{H_1}^i = \sum_{n=j}^{k} \prod_{m=j}^{n-1} (1 - P_{H_1}(t_m)) P_{H_1}(t_n) \qquad (10)$$

where $P_{H_1}^i$ is the prior probability of at least one measurement fault in the measurement batch for the i^{th} satellite. $P_{H_1}(t_m)$ and $P_{H_1}(t_n)$ are the state probabilities of satellite failure at the measurement time t_m and t_n respectively. The details of computing $P_{H_1}(t_m)$ and $P_{H_1}(t_n)$ are also shown in Appendix D.

Vertical requirements to meet LPV-200, which are more demanding that the horizontal requirements for precision approach, are assumed to compute the system VPL. A 35 meter vertical alert limit (VAL) is also assumed in compliance with LPV-200 requirements. In addition, VPLs for batch-equivalent smoothed code positioning integrity are also computed using the algorithm that generates a RAIM based VPL in the GEAS ARAIM architecture [7].

Fig. 4 shows VPL results for four different systems based the aforementioned simulation scenario. These systems are a 1000-second smoothed code positioning process, a 30-minute batch estimator without receiver clock aiding, a 30-minute batch estimator with chip-scale atomic clock aiding and the same estimator with rubidium atomic clock aiding. The results show that a batch estimator with good-quality receiver clock aiding can significantly reduce VPL peaks caused by bad geometries, which are the areas at both ends in Fig.4. Figures 5 to 6 display the details of the VPL peak areas in Fig. 4. We can observe that the rubidium receiver clock aiding can help the system coast through these two bad-geometry areas without violating the vertical integrity requirements. It performs best among all systems, which was expected. The chip-scale atomic receiver clock aiding performs much better than the standalone batch estimator in the first area, but its performance is similar to the standalone batch estimator in the second area. The

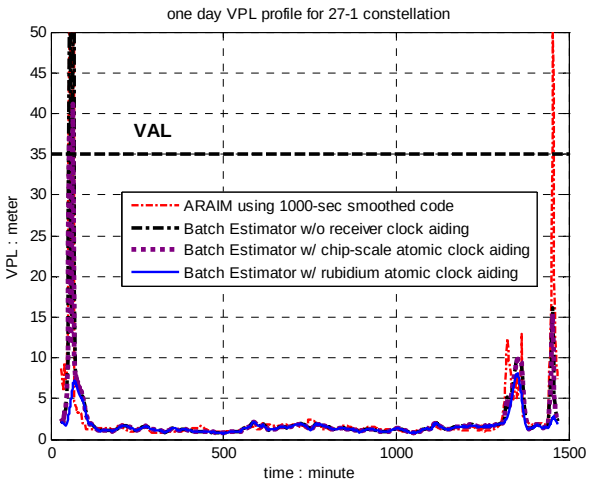

Figure 4. System integrity performance comparison

integrity improvement of the chip-scale atomic aiding is expected to be lower (because of low clock quality) than the rubidium receiver clock aiding. Finally, the standalone batch estimator performs better than its smoothed-code-positioning counterpart because of the better accuracy provided by the batch estimation.

Although a lower-quality receiver clock provides much less help in improving system availability (as shown in Fig. 5), it still has great potential to improve system continuity. This is especially true for unexpected and severe SV blockages, such as those caused by aircraft banking. Fig. 7 displays VPL results for an extreme example with only four satellites available during partial blockage. In this case, there is no fault detection function available if the system has no receiver clock aiding (five or more SVs needed). However, the batch estimator with chip-sale atomic receiver clock aiding can help the system coast through a 200 second period for this severe blockage case. The rubidium receiver clock aiding can maintain the system integrity much longer, over a 30 minute period in this example.

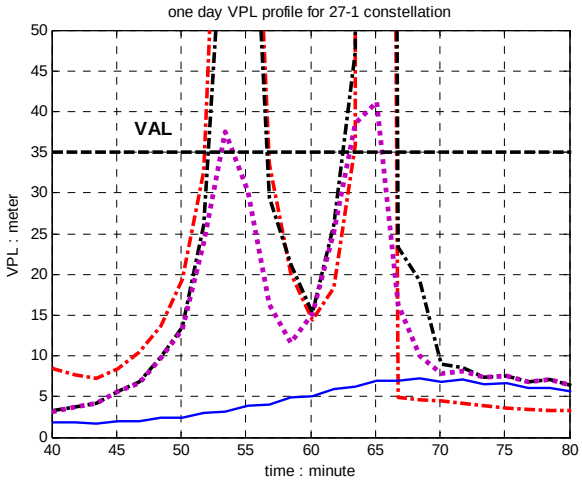

Figure 5. VPL reduction in the first peak area

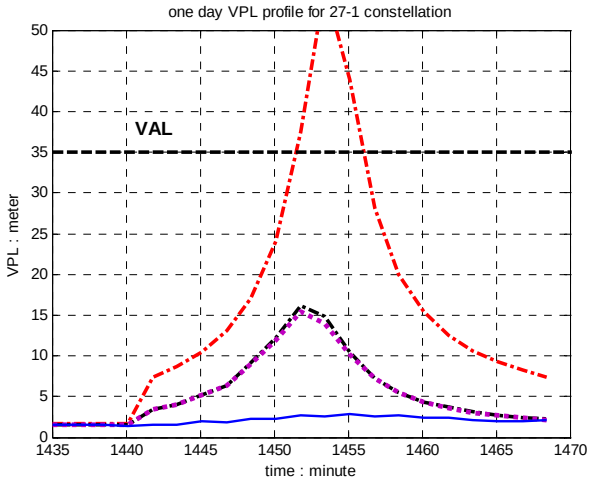

Figure 6. VPL reduction in the second peak area

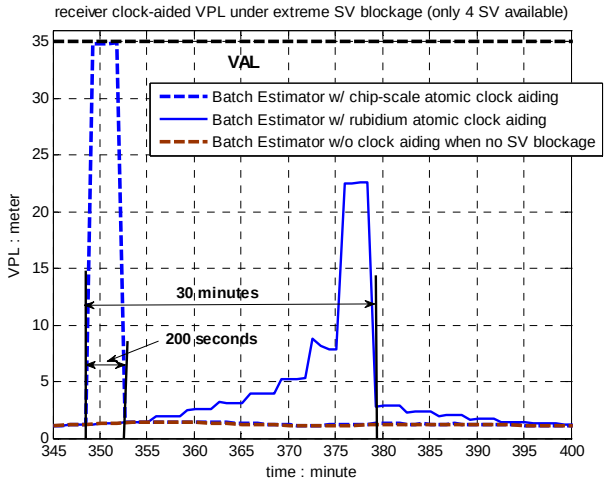

Figure 7. Continuity improvement from receiver clock aiding

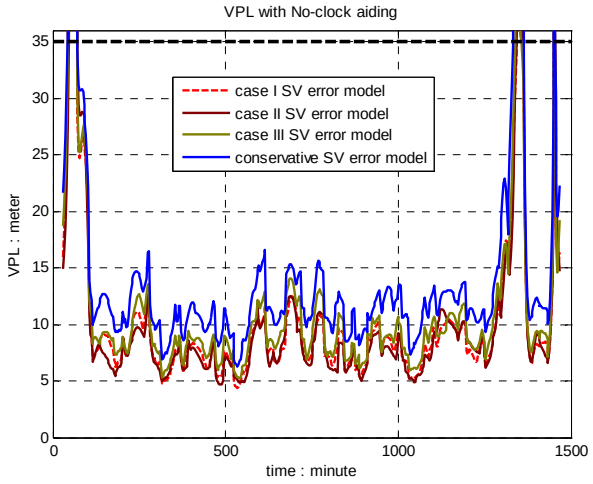

Figure 8. Wost VPL for conservative satellite error model

Up to now, we have investigated specific cases to show how the batch estimation and receiver clock aiding help to improve accuracy and integrity. The performance of the receiver clock-aided system for real applications is evaluated for real applications in the next section.

VI. Global Coverage Performance for Receiver Clock-Aided Navigation System

To understand the performance of the batch estimator with receiver clock aiding for real applications, the GEAS ARAIM architecture is adopted to evaluate the system performance. GEAS was defined and studied by the FAA to evaluate potential navigation architectures for global aircraft precision approach capability (LPV-200 [8]) using modernized dual frequency (L1/L5) GPS measurements. In this investigation, the vertical position requirements to meet LPV-200 aircraft precision approach standards are considered. All GEAS error models are adopted in the performance simulation for the receiver clock-aided navigation system, except the satellite ephemeris and clock error model [7].

A. Satellite Clock and Ephemeris Error Model for Batch Estimation

In GEAS, a 0.5 m standard deviation bound (URA) on satellite clock and ephemeris error with 10^{-5} integrity risk is used. However, an 8.5×10^{-4} m/sec satellite clock and ephemeris error rate is also assumed, which would lead to a satellite clock/ephemeris coasting error larger then URA in 10 minutes. However, the current GPS ephemeris is normally updated every two hours.

TABLE II. BOUNDARY AND CONSERVATIVE SV ERROR MODELS

	Initial error offset: m	Initial error rate offset: m/sec	Correlation
Case I Model	0.2	$1x10^{-4}$	0
Case II Model	0.5	$1x10^{-4}$	-0.95
Case III Model	0.2	$1x10^{-4}$	-0.95
Conservative Model	0.5	$2x10^{-4}$	0

To address this issue, a linear SV error model which is composed of an initial error offset (in meters) and an initial error rate offset (in m/sec) is investigated. The SV error model with different initial errors and error rates was analyzed with positive and negative correlations between the initial error offset and error rate. Based on these analyses, the performance for three boundary cases, which are consistent with a 0.5 m URA for satellite clock/ephemeris error over a two hour period, is simulated. Then, a linear model is selected to be more conservative than all three boundary cases. Models for the boundary cases and the conservative model are listed in Table II and simulated VPL results are shown in Fig. 8. The blue VPL curve using the conservative model is above the other three VPL curves in the figure.

The satellite clock-phase random coasting error is negligible in satellite clock/ephemeris error model due to its small magnitude compared to the error from the conservative linear error model.

B. System Performance Evaluation for LVP-200 Application

Since the future GPS III constellation is most likely to have 27 SVs, four future possible GPS III constellations considered in GEAS are used here to simulate the receiver clock-aided navigation system performance. These four constellations are 24 and 24-minus-1 constellations, and 27 and 27-minus-1 constellations. The geometry sampling period is 3 minutes. The navigation system structure is the same as in previously analyzed cases: a moving window batch estimator with or without receiver clock adding is implemented with a 30 minute batch interval. Measurements sampled at infrequent intervals (every 200 seconds) in the batch include 100-second smoothed code and carrier measurements. The simulated performance is shown in Table III in terms of global coverage of 99.5% LVP-200 availability. A 5 deg by 5 deg latitude-longitude grid locations with latitudes ranging from N 70 deg to S 70 deg and longitudes ranging from E 180 deg to W 180 deg is used to establish global system performance.

TABLE III. RECEIVER CLOCK-AIDED NAVIGATION SYSTEM PERFORMANCE

	Global Coverage: %			
	24-1	***24***	***27-1***	***27***
Batch Estimator (BE) only	63.8	98.1	91.1	100
BE w/ chip-scale atomic clock aiding	65.4	98.2	91.4	100
BE w/ rubidium clock aiding	99.6	100	100	100

In Table III, the first row is the performance of the batch estimator only. We can see that it only reaches 100% global coverage for the 27 constellation. The second row is the results of the batch estimator with chip-scale atomic clock aiding. The system performance is similar to that of the batch estimator only, with some improvement for the 24-1 constellation. The bottom row is the performance of the batch estimator with rubidium clock aiding. The system achieves 100% global coverage for all constellations except 24-1. In general, the performance for receiver clock-aided batch estimator algorithm shows a great potential in improving system availability.

VII. SUMMARY AND FUTURE WORK

In this work, the time correlation of receiver clock-phase random coasting errors has been analytically verified using a previously validated clock random phase variance equation. A complete time correlation matrix for a sequence of clock random errors has been derived.

A batch estimator that fully accounts for the receiver clock random errors and their time correlation has been developed to ensure error modeling integrity of a clock-aided navigation system.

Improvements in position accuracy and fault detection performance have been fully investigated using the batch estimator. Reduction in VPL peak values has been demonstrated for the receiver clock-aided system, resulting in significant potential improvement in system availability.

A benchmark LPV-200 application based on the GEAS ARAIM architecture was adopted to illustrate the performance of the high-integrity receiver clock-aided system. Global coverage results are promising even in cases of poor satellite geometry.

In future work, the receiver clock-aided navigation system performance will be verified using experimental data.

ACKNOWLEDGMENT

The authors would like to express their appreciation to the FAA Satellite Navigation Program Office for supporting this work. And many thanks to the colleagues in the IIT NavLab for their advice

REFERENCE

[1] Misra, P., Pratt, M., Burke, B. and Ferranti, R., "Adaptive Modeling of Receiver Clock for Meter-Level DGPS Vertical Positioning," Proceedings of the ION GPS-95, Palm Springs, CA, September 1995

[2] Brown, R. G. and Hwang, P. Y. C., Introduction to Random Signals and Applied Kalman Filtering, John Wiley & Sons, New York.

[3] Van Dierendonck, A. J. and Brown, R. G., "Relationship between Allan Variances and Kalman Filter Parameters," Proceedings of the Precise Time and Time Interval (PTTI) Systems and Applications, Category 5, Vol. 29.

[4] Fang-C. Chan and Boris Pervan, " Stochastic Modeling of GPS Receiver Clocks for Improved Positioning and Fault Detection Performance," Proceedings of the 22nd International Technical Meeting of the Satellite Division of the Institute of Navigation (ION GNSS-2009), Savannah, GA, September 22-25, 2009.

[5] Lee, Y. C. and McLaughlin, M. P. "Feasibility Analysis of RAIM to Provide LPV-200 Approaches with Future GPS," ION GNSS 20th International Technical Meeting of the Satellite Division, Sep. 2007, Fort Worth, TX.

[6] Blanch, J., Ene, A. Walter, T. and Enge P., "An Optimized Multiple Hypothesis RAIM Algorithm for Vertical Guidance," ION GNSS 20th International Technical Meeting of the Satellite Division, Sep. 2007, Fort Worth, TX.

[7] Walter, T., Enge, P., Blanch, J. and Pervan, B., "Worldwide Vertical Guidance of Aircraft Based on Modernized GPS and New Integrity Augmentations" Proceedings of the IEEE, Vol. 96, Issue 12, Dec. 2008

[8] "Program Requirements for the Wide Area Augmentation System (WAAS)," FAA doc. WAAS070030, Jun. 5 2007

[9] Vernotte, F., Delporte, J., Brunet, M. and Tournier, T., "Uncertainties of drift coefficients and extrapolation errors: Application to clock error prediction," Metrologia, Vol. 38, No. 4, 2001.

[10] S. Knappe, P.D.D. Schwindt, V. Shah, L. Hollberg, and J. Kitching, "A chip-scale atomic clock based on 87Rb with improved frequency stability," OPTICS EXPRESS, Vol. 13, No. 4, 2005

APPENDIX

Appendix A

In this Appendix, the equation for the time correlation of clock random phase errors [3] is re-visited, starting with the power spectrum equation for the three clock frequency error sources shown in (2):

$$S_f(f) = h_0 f^0 + h_{-1} f^{-1} + h_{-2} f^{-2} \tag{a.1}$$

Each error source can be modeled as unit white noise passing through a transfer function in the Laplace domain ('*s*' domain), and its contribution to the clock-phase random coasting error is the time integral of the resulting inverse Laplace function. The equations that transfer the white noise into clock-phase random errors for the three error sources are respectively expressed as:

$$\begin{aligned} H_{\delta\theta_0}(s) &= \sqrt{h_0 / 2s^2} \\ H_{\delta\theta_{-1}}(s) &= \sqrt{\pi h_{-1} / s^3} \\ H_{\delta\theta_{-2}}(s) &= \sqrt{2\pi^2 h_{-2} / s^4} \end{aligned} \tag{a.2}$$

Three impulse response functions are obtained for the transfer functions above. The clock-phase random errors can be modeled in the time domain by the time convolutions of the unit driving white noise (n_0, n_{-1} and n_{-2}) with the impulse response functions ($h_{\delta\theta_0}$, $h_{\delta\theta-1}$ and $h_{\delta\theta_{-2}}$).

$$
\begin{aligned}
&h_{\delta\theta_0}(t) = \sqrt{h_0/2} \Rightarrow \delta\theta_0(t) = \int_0^t h_{\delta\theta_0}(u) n_0(t-u)du \\
&h_{\delta\theta_{-1}}(t) = 2\sqrt{h_{-1}t} \Rightarrow \delta\theta_{-1}(t) = \int_0^t h_{\delta\theta_{-1}}(u) n_{-1}(t-u)du \\
&h_{\delta\theta_{-2}}(t) = t\sqrt{2\pi^2 h_{-2}} \Rightarrow \delta\theta_{-2}(t) = \int_0^t h_{\delta\theta_{-2}}(u) n_{-2}(t-u)du
\end{aligned}
\tag{a.3}
$$

The time correlation of clock-phase random coasting errors between coasting times Δt_i and Δt_j is given by:

$$
\begin{aligned}
&R_{\delta\theta}(\Delta t_i, \Delta t_j) = E[\delta\theta(\Delta t_i)\delta\theta(\Delta t_j)] \\
&= E[(\delta\theta_0(\Delta t_i) + \delta\theta_{-1}(\Delta t_i) + \delta\theta_{-2}(\Delta t_i)) \times \\
&\quad (\delta\theta_0(\Delta t_j) + \delta\theta_{-1}(\Delta t_j) + \delta\theta_{-2}(\Delta t_j))]
\end{aligned}
\tag{a.4}
$$

Since there is no correlation between each individual white error sources, equation (a.4) can be re-written as:

$$
\begin{aligned}
&R_{\delta\theta}(\Delta t_i, \Delta t_j) \\
&= E[(\delta\theta_0(\Delta t_i)\delta\theta_0(\Delta t_j) + \delta\theta_{-1}(\Delta t_i)\delta\theta_{-1}(\Delta t_j) \\
&+ \delta\theta_{-2}(\Delta t_i)\delta\theta_{-2}(\Delta t_j))]
\end{aligned}
\tag{a.5}
$$

A general formula for the auto correlation of the clock-phase random coasting error contribution from one frequency error source x (with driving white noise n_x and impulse response function h_x) between time t_1 and t_2 is given by:

$$
\begin{aligned}
&R_{xx}(t_1, t_2) \equiv E[x(t_1)x(t_2)] \\
&= E\left[\int_0^{t_1} h_x(u) n_x(t_1-u)du \int_0^{t_2} h_x(v) n_x(t_2-v)dv\right] \\
&= \int_0^{t_1}\int_0^{t_2} h_x(u)h_x(v)E[n_x(t_1-u)n_x(t_2-v)]dudv \\
&= \int_0^{t_1}\int_0^{t_2} h_x(u)h_x(v)\delta(u-v+t_2-t_1)dudv \\
&= \int_0^{t_1} h_x(u)h_x(u+(t_2-t_1))du
\end{aligned}
\tag{a.6}
$$

Applying equation (a.6) to the auto correlation terms in equation (a.5), the auto correlation of each phase random error is expressed as:

$$
\begin{aligned}
&R_{\delta\theta_0}(\Delta t_i, \Delta t_j) = E[(\delta\theta_0(\Delta t_i)\delta\theta_0(\Delta t_j)] \\
&= \int_0^{\Delta t_i} \sqrt{h_0/2}\sqrt{h_0/2}du \\
&= \frac{h_0}{2}\Delta t_i
\end{aligned}
\tag{a.7}
$$

$$
\begin{aligned}
&R_{\delta\theta_{-1}}(\Delta t_i, \Delta t_j) = E[(\delta\theta_{-1}(\Delta t_i)\delta\theta_{-1}(\Delta t_j)] \\
&= \int_0^{\Delta t_i} 2\sqrt{h_{-1}u}\,2\sqrt{h_{-1}(u+(\Delta t_j - \Delta t_i))}du \\
&= 4h_{-1}\int_0^{\Delta t_i}\sqrt{u(u+(\Delta t_j - \Delta t_i))}du \\
&= h_{-1}[(\Delta t_i + \Delta t_j)\sqrt{\Delta t_i \Delta t_j} \\
&\quad -(\Delta t_j - \Delta t_i)^2 \ln\left|\frac{\sqrt{\Delta t_i}+\sqrt{\Delta t_j}}{\sqrt{(\Delta t_j - \Delta t_i)}}\right|]
\end{aligned}
\tag{a.8}
$$

$$
\begin{aligned}
&R_{\delta\theta_{-2}}(\Delta t_i, \Delta t_j) = E[(\delta\theta_{-2}(\Delta t_i)\delta\theta_{-2}(\Delta t_j)] \\
&= \int_0^{\Delta t_i}\sqrt{2\pi^2 h_{-2}}u\sqrt{2\pi^2 h_{-2}}(u+(\Delta t_j - \Delta t_i))du \\
&= 2\pi^2 h_{-2}\left(\frac{\Delta t_i^{\,3}}{3} + \frac{\Delta t_i^{\,2}}{2}(\Delta t_j - \Delta t_i)\right)
\end{aligned}
\tag{a.9}
$$

Equations (a.7)-(a.9) are used in (4). When the coasting time $\Delta t_i = \Delta t_j$, the equation (a.5) results in the same as equation (3).

Appendix B

Direct measurements on clock phase with white measurement noise is assumed, a batch of clock measurements can be formed based on (1):

$$
\begin{aligned}
m_0 &= \Delta\theta_0 + v_0 \\
m_1 &= \Delta\theta_0 + \Delta t \cdot \Delta f_0 + \delta\theta_1 + v_1 \\
m_2 &= \Delta\theta_0 + 2\Delta t \cdot \Delta f_0 + \delta\theta_2 + v_2 \\
&\vdots \\
m_k &= \Delta\theta_0 + k\Delta t \cdot \Delta f_0 + \delta\theta_k + v_k
\end{aligned}
\tag{b.1}
$$

where $\Delta\theta_0$ and Δf_0 are the initial clock phase and frequency offsets. The measurement noise v_k of measurement m_k at epoch time k is assumed uncorrelated in time. Δt is the sampling interval and $\delta\theta_k$ is the clock-phase random error at time epoch k.

A batch measurement equation for this simple example can be constructed as:

$$
\begin{bmatrix} m_0 \\ m_1 \\ \vdots \\ m_k \\ 0 \\ 0 \\ \vdots \\ 0 \\ 0 \end{bmatrix} =
\begin{bmatrix}
1 & 0 & 0 & \cdots & \cdots & 0 & 0 \\
1 & \Delta t & 1 & \cdots & \cdots & 0 & 0 \\
\vdots & \vdots & \vdots & & & \vdots & \vdots \\
1 & k\Delta t & 0 & & \cdots & 0 & 1 \\
\hline
1 & 0 & \cdots & & & \cdots & 0 \\
0 & 1 & & & & & \\
\vdots & & & \ddots & & & \vdots \\
 & & & & & 1 & 0 \\
0 & \cdots & & & \cdots & 0 & 1
\end{bmatrix}
\begin{bmatrix} \Delta\theta_0 \\ \Delta f_0 \\ \delta\theta_1 \\ \delta\theta_2 \\ \vdots \\ \delta\theta_{k-1} \\ \delta\theta_k \end{bmatrix} +
\begin{bmatrix} v_0 \\ v_1 \\ \vdots \\ v_k \\ w_{\delta\theta_1} \\ w_{\delta\theta_2} \\ \vdots \\ w_{\delta\theta_{k-1}} \\ w_{\delta\theta_k} \end{bmatrix}
\tag{b.2}
$$

where $w_{\delta\theta_k}$ is the modeled uncertainty on the pseudo-measurement for clock-phase random error $\delta\theta_k$.

Equation (b.2) takes the form:

$$\vec{m}_{BE} = H_{BE}\vec{s}_{BE} + \vec{v}_{BE} \tag{b.3}$$

The measurement vector $\vec{m}_{BE}$, observation matrix H_{BE} and measurement noise vector $\vec{v}_{BE}$ in (b.2) are all made of two parts (separated by a horizontal line for clarity of explanation). For the observation matrix, the upper part is the matrix constructed using (b.1), and the lower part is an indentity matrix used to incorporate direct pseudo-measurements of the state vector $\vec{s}_{BE}$. The states are the initial clock phase and frequency offsets and the clock random errors. Because these states are assumed zero-mean Gaussian distributed, best guess values of the pseudo-measurements are zeros. As for the measurement noise vector, the upper part corresponds to the white measurement noise, and the lower part is used to express uncertainties on the pseudo-measurements. These uncertainties on the pseudo-measurements account for prior knowledge of the initial clock phase and frequency offsets, and for the clock random error whose dynamics must be modeled over time.

The least squares estimation of the states $\vec{s}_{BE}$ is:

$$\vec{s}_{BE} = (H_{BE}{}^T V_{BE}{}^{-1} H_{BE}) H_{BE}{}^T V_{BE}{}^{-1} \vec{m}_{BE} \tag{b.4}$$

where the inverse of the weighting matrix $V_{BE}{}^{-1}$ is:

$$V_{BE} = \mathrm{cov}(\vec{v}_{BE}) = \begin{bmatrix} \mathrm{cov}(v) & 0 & 0 \\ 0 & P_0 & 0 \\ 0 & 0 & W_{\delta\theta}(\Delta t \to k\Delta t) \end{bmatrix} \tag{b.5}$$

The first block matrix $\mathrm{cov}(v)$ on the diagonal of V_{BE} is the covariance of the white measurement noise. The second block matrix P_0 is the prior knowledge on the initial clock-phase and frequency offsets. The last block matrix $W_{\delta\theta}(\Delta t \to k\Delta t)$ on the diagonal of V_{BE} is the complete covariance matrix (including all time correlation terms) that was derived in the previous section and expressed in (5) and (8). We show the results here again:

$$W_{\delta\theta}(\Delta t \to k\Delta t) = \begin{bmatrix} R_{\delta\theta}(\Delta t, \Delta t) & R_{\delta\theta}(\Delta t, 2\Delta t) & \cdots & R_{\delta\theta}(\Delta t, k\Delta t) \\ R_{\delta\theta}(2\Delta t, \Delta t) & R_{\delta\theta}(2\Delta t, 2\Delta t) & & \vdots \\ \vdots & & \ddots & \vdots \\ R_{\delta\theta}(k\Delta t, \Delta t) & \cdots & \cdots & R_{\delta\theta}(k\Delta t, k\Delta t) \end{bmatrix}$$

In parallel, a traditional two-state Kalman filter [2] for clock phase and frequency estimation can be shown as:

a) state initialization:

$$\bar{s}_0 = \begin{bmatrix} b_0 & f_0 \end{bmatrix}^T, P_0 = \mathrm{cov}(\bar{s}_0) \tag{b.6}$$

b) measurement model:

$$m_k = \begin{bmatrix} 1 & 0 \end{bmatrix} \bar{s}_k + v_k = b_k + v_k \tag{b.7}$$

c) state propagation in time:

$$\begin{aligned} \bar{s}_{k+1} &= \begin{bmatrix} 1 & \Delta t \\ 0 & 1 \end{bmatrix} \bar{s}_k + \vec{w}_k \\ \vec{w}_k &= \begin{bmatrix} w_{b_k} \\ w_{f_k} \end{bmatrix}, \ \mathrm{cov}(\vec{w}_k) = W_{\delta\theta,\delta f}(\Delta t) \end{aligned} \tag{b.8}$$

where $\bar{s}_k$ is the clock state at time epoch k, b_k and f_k are the clock phase and frequency components in the clock state. m_k and v_k are the measurement and white measurement noise respectively. $\vec{w}_k$ is the clock process noise vector, which is zero mean for phase and frequency components w_{b_k} and w_{f_k}. The covariance of $\vec{w}_k$ is the matrix used in a traditional Kalman filter to account for the uncertainties on clock phase and frequency time propagation.

The following steps aim at deriving a batch estimator equivalent to the Kalman filter. The clock frequency state at any epoch can be traced back to the initial clock frequency state (f_0) and some combination of the clock process noise vectors at previous epochs using the state transition matrix shown in (b.8):

$$\begin{aligned} f_1 &= f_0 + w_{f_1} \\ f_2 &= f_1 + w_{f_2} \\ &= f_0 + w_{f_1} + w_{f_2} \\ &\vdots \\ f_k &= f_0 + w_{f_1} + w_{f_2} + \cdots w_{f_k} \end{aligned} \tag{b.9}$$

Similar derivation is performed for the clock phase states:

$$
\begin{aligned}
b_1 &= b_0 + \Delta t \cdot f_0 + w_{b_1} \\
b_2 &= b_1 + \Delta t \cdot f_1 + w_{b_2} \\
&= b_0 + \Delta t \cdot f_0 + w_{b_1} + \Delta t \cdot f_1 + w_{b_2} \\
&= b_0 + \Delta t \cdot f_0 + w_{b_1} + \Delta t \cdot (f_0 + w_{f_1}) + w_{b_2} \\
&= b_0 + 2\Delta t \cdot f_0 + \Delta t \cdot w_{f_1} + w_{b_1} + w_{b_2} \\
&\vdots \\
b_k &= b_0 + k\Delta t \cdot f_0 + (k-1)\Delta t \cdot w_{f_1} + \cdots + \Delta t \cdot w_{f_{k-1}} \\
&\quad + w_{b_1} + w_{b_2} + \cdots w_{b_k}
\end{aligned}
\tag{b.10}
$$

We can substitute the phase component b_k in (b.7) with the relationship derived in (b.10). A batch of measurements from epoch *0* to *k* can be formed:

$$
\begin{aligned}
m_0 &= b_0 + v_0 \\
m_1 &= b_0 + \Delta t \cdot f_0 + w_{b_1} + v_1 \\
m_2 &= b_0 + 2\Delta t \cdot f_0 + \Delta t \cdot w_{f_1} + w_{b_1} + w_{b_2} + v_2 \\
&\vdots \\
m_k &= b_0 + k\Delta t \cdot f_0 + (k-1)\Delta t \cdot w_{f_1} + \cdots + \Delta t \cdot w_{f_{k-1}} \\
&\quad + w_{b_1} + w_{b_2} + \cdots w_{b_k} + v_k
\end{aligned}
\tag{b.11}
$$

Therefore, a batch measurement equation can be constructed using (b.11):

$$
\begin{bmatrix} m_0 \\ m_1 \\ \vdots \\ m_k \\ \hline 0 \\ 0 \\ \vdots \\ 0 \\ 0 \end{bmatrix}
=
\left[\begin{array}{ccccccc}
1 & 0 & 0 & \cdots & \cdots & 0 & 0 \\
1 & \Delta t & 0 & \cdots & \cdots & 0 & 0 \\
\vdots & \vdots & \vdots & & & \vdots & \vdots \\
1 & k\Delta t & 1 & (k-1)\Delta t & \cdots & 1 & 0 \\
\hline
 & 1 & 0 & \cdots & & \cdots & 0 \\
 & 0 & 1 & & & & \\
 & \vdots & & \ddots & & & \vdots \\
 & & & & & 1 & 0 \\
 & 0 & \cdots & & \cdots & 0 & 1
\end{array}\right]
\begin{bmatrix} b_0 \\ f_0 \\ w_{b_1} \\ w_{f_1} \\ \vdots \\ w_{b_k} \\ w_{f_k} \end{bmatrix}
+
\begin{bmatrix} v_0 \\ v_1 \\ \vdots \\ v_k \\ \hline w_{b_1} \\ w_{f_1} \\ \vdots \\ w_{b_k} \\ w_{f_k} \end{bmatrix}
\tag{b.12}
$$

Similar to the batch equation in (b.2), the matrices in (b.12) are made of two parts (separated by a horizontal line). The upper part is (b.11) expressed in matrix form, and the lower part comprises the pseudo-measurements for the initial clock-phase and frequency offsets and clock process noise vectors. Best guesses of the pseudo-measurement values are zeros. Equation (b.12) is written in the form:

$$
\vec{m}_{KF} = H_{KF}\vec{s}_{KF} + \vec{v}_{KF} \tag{b.13}
$$

The least squares estimation of the state vector $\vec{s}_{KF}$ is given by:

$$
\vec{s}_{KF} = ({H_{KF}}^T {V_{KF}}^{-1} H_{KF}) {H_{KF}}^T {V_{KF}}^{-1} \vec{m}_{KF} \tag{b.14}
$$

where the inverse of the weighting matrix ${V_{KF}}^{-1}$ is:

$$
V_{KF} = \mathrm{cov}(\vec{v}_{KF}) = \begin{bmatrix} \mathrm{cov}(v) & 0 & 0 \\ 0 & P_0 & 0 \\ 0 & 0 & W_{\delta\theta,\delta f}(\Delta t \to k\Delta t) \end{bmatrix} \tag{b.15}
$$

The first block matrix $\mathrm{cov}(v)$ on the diagonal of V_{KF} is the covariance of the white measurement noise. The second block matrix P_0 is the prior knowledge on the initial clock-phase and frequency offsets expressed in (b.6). The last block matrix $W_{\delta\theta,\delta f}(\Delta t \to k\Delta t)$ is composed of the *k* clock process noise matrices used in the Kalman filter time propagation:

$$
\begin{aligned}
&W_{\delta\theta,\delta f}(\Delta t \to k\Delta t) \\
&= \begin{bmatrix} W_{\delta\theta,\delta f}(\Delta t) & 0 & \cdots & 0 \\ 0 & W_{\delta\theta,\delta f}(\Delta t) & & \vdots \\ \vdots & & \ddots & \vdots \\ 0 & \cdots & \cdots & W_{\delta\theta,\delta f}(\Delta t) \end{bmatrix}
\end{aligned}
\tag{b.16}
$$

where $W_{\delta\theta,\delta f}(\Delta t)$ is the clock process noise matrix expressed in (b.8), the derivation of $W_{\delta\theta,\delta f}(\Delta t)$ can be found in [2] [3]. A numerical simulation can be performed to show that clock estimations using the Kalman filter in (b.6)-(b.8) matches results obtained from the equivalent batch estimator in (b.12)-(b.16).

Appendix C

A smoothed code measurement generated through a Hatch filter is computed using the following equation:

$$
\begin{aligned}
\bar{\rho}_k &= \frac{1}{\alpha}\rho_k + \frac{\alpha - 1}{\alpha}(\bar{\rho}_{k-1} + \phi_k - \phi_{k-1}) \\
\alpha &= \frac{t_{sm}}{\Delta t}
\end{aligned}
\tag{c.1}
$$

where $\bar{\rho}_k$ is the smoothed code measurement at epoch *k*, ρ_k is the raw code measurement at epoch k, ϕ_k and ϕ_{k-1} are the raw carrier measurements at epochs *k* and *k-1* respectively. α is the total number of measurements included within the smoothing time interval t_{sm} with sampling period Δt.

We consider multipath as the only measurement error source, and use $\varepsilon_{\bar{\rho},k}$, $\varepsilon_{\rho,k}$ and $\varepsilon_{\phi,k}$ to represent smoothed code, raw code and raw carrier multipath errors at epoch *k*. Using (c.1), the smoothed code multipath at epoch *k* can be expressed as:

$$
\varepsilon_{\bar{\rho},k} = \frac{1}{\alpha}\varepsilon_{\rho,k} + \frac{\alpha - 1}{\alpha}(\varepsilon_{\bar{\rho},k-1} + \varepsilon_{\phi,k} - \varepsilon_{\phi,k-1}) \tag{c.2}
$$

The multipath error is modeled as a first order Markov process:

$$\begin{aligned}\varepsilon_{\rho,k} &= \beta_1 \varepsilon_{\rho,k-1} + v_{\rho,k} \\ \varepsilon_{\phi,k} &= \beta_2 \varepsilon_{\phi,k-1} + v_{\phi,k}\end{aligned} \tag{c.3}$$

where β_1 and β_2 are the correlation coefficients for raw code and carrier multipath errors correspondingly. $v_{\rho,k}$ and $v_{\phi,k}$ are the driving white noise.

At a steady state, the variances of the raw code and carrier multipath errors are:

$$\begin{aligned}E[\varepsilon_{\rho,k}^2] &= E[\varepsilon_{\rho,k-1}^2] = \sigma_\rho^2 \\ E[\varepsilon_{\phi,k}^2] &= E[\varepsilon_{\phi,k-1}^2] = \sigma_\phi^2\end{aligned} \tag{c.4}$$

The time correlation between carrier multipath errors at epochs *k* and *k-1* can be derived at steady state:

$$\begin{aligned}&E[\varepsilon_{\phi,k}\varepsilon_{\phi,k-1}] = E[(\beta_2 \varepsilon_{\phi,k-1} + v_{\phi,k})\varepsilon_{\phi,k-1}] \\ &= \beta_2 E[\varepsilon_{\phi,k-1}\varepsilon_{\phi,k-1}] + E[\varepsilon_{\phi,k-1} v_{\phi,k}] = \beta_2 \sigma_\phi^2\end{aligned} \tag{c.5}$$

Therefore, the correlation between smoothed code and carrier multipath errors can be derived:

$$\begin{aligned}&E[\varepsilon_{\bar{\rho},k}\varepsilon_{\phi,k}] \\ &= E[(\frac{1}{\alpha}\varepsilon_{\rho,k} + \frac{\alpha-1}{\alpha}(\varepsilon_{\bar{\rho},k-1} + \varepsilon_{\phi,k} - \varepsilon_{\phi,k-1}))\varepsilon_{\phi,k}] \\ &= \frac{1}{\alpha}E[\varepsilon_{\rho,k}\varepsilon_{\phi,k}] + \frac{\alpha-1}{\alpha}E[\varepsilon_{\bar{\rho},k-1}\varepsilon_{\phi,k}] \\ &+ \frac{\alpha-1}{\alpha}(E[\varepsilon_{\phi,k}\varepsilon_{\phi,k}] - E[\varepsilon_{\phi,k}\varepsilon_{\phi,k-1}])\end{aligned}$$

Assuming zero correlation between raw code and carrier multipath error, the first term is zero. Substitute $\varepsilon_{\phi,k}$ using (c.3) and $E[\varepsilon_{\phi,k}\varepsilon_{\phi,k-1}]$ using (c.5), the above equation is re-written as:

$$\begin{aligned}&E[\varepsilon_{\bar{\rho},k}\varepsilon_{\phi,k}] \\ &= \frac{\alpha-1}{\alpha}(\beta_2 E[\varepsilon_{\bar{\rho},k-1}\varepsilon_{\phi,k-1}] + E[\varepsilon_{\phi,k}\varepsilon_{\phi,k}] - \beta_2\sigma_\phi^2)\end{aligned}$$

Since we are considering the steady state condition, all time indexes can be dropped. Therefore, the correlation can be obtained:

$$\begin{aligned}E[\varepsilon_{\bar{\rho}}\varepsilon_{\phi}] &= \frac{\alpha-1}{\alpha}(\beta_2 E[\varepsilon_{\bar{\rho}}\varepsilon_{\phi}] + \sigma_\phi^2 - \beta_2\sigma_\phi^2) \\ &= \frac{\alpha-1}{\alpha}\beta_2 E[\varepsilon_{\bar{\rho}}\varepsilon_{\phi}] + \frac{\alpha-1}{\alpha}(1-\beta_2)\sigma_\phi^2 \\ &\Rightarrow (1-\frac{\alpha-1}{\alpha}\beta_2)E[\varepsilon_{\bar{\rho}}\varepsilon_{\phi}] = \frac{\alpha-1}{\alpha}(1-\beta_2)\sigma_\phi^2\end{aligned}$$

$$E[\varepsilon_{\bar{\rho}}\varepsilon_{\phi}] = \frac{\alpha-\alpha\beta_2-1+\beta_2}{\alpha-\alpha\beta_2+\beta_2}\sigma_\phi^2 \tag{c.6}$$

Before the derivation of the steady state standard deviation of smoothed code measurement, the time correlation between the smoothed code and the raw code measurement at steady state has to be obtained:

$$\begin{aligned}&E[\varepsilon_{\bar{\rho},k}\varepsilon_{\rho,k}] \\ &= E[(\frac{1}{\alpha}\varepsilon_{\rho,k} + \frac{\alpha-1}{\alpha}(\varepsilon_{\bar{\rho},k-1} + \varepsilon_{\phi,k} - \varepsilon_{\phi,k-1}))\varepsilon_{\rho,k}] \\ &= \frac{1}{\alpha}E[\varepsilon_{\rho,k}\varepsilon_{\rho,k}] + \frac{\alpha-1}{\alpha}(E[\varepsilon_{\bar{\rho},k-1}\varepsilon_{\rho,k}] + E[(\varepsilon_{\phi,k} - \varepsilon_{\phi,k-1})\varepsilon_{\rho,k}]) \\ &= \frac{1}{\alpha}E[\varepsilon_{\rho,k}\varepsilon_{\rho,k}] + \frac{\alpha-1}{\alpha}\beta_1 E[\varepsilon_{\bar{\rho},k-1}\varepsilon_{\rho,k-1}] \\ &+ \frac{\alpha-1}{\alpha}(E[\varepsilon_{\bar{\rho},k-1}v_{\rho,k}] + E[(\varepsilon_{\phi,k} - \varepsilon_{\phi,k-1})\varepsilon_{\rho,k}])\end{aligned}$$

The last two terms are zero because they are not correlated, and the time indexes can also be dropped at steady state. The correlation can be re-written as:

$$\begin{aligned}E[\varepsilon_{\bar{\rho}}\varepsilon_{\rho}] &= \frac{1}{\alpha}E[\varepsilon_{\rho}\varepsilon_{\rho}] + \frac{\alpha-1}{\alpha}\beta_1 E[\varepsilon_{\bar{\rho}}\varepsilon_{\rho}] \\ &\Rightarrow (1-\frac{\alpha-1}{\alpha}\beta_1)E[\varepsilon_{\bar{\rho}}\varepsilon_{\rho}] = \frac{1}{\alpha}\sigma_\rho^2\end{aligned}$$

$$E[\varepsilon_{\bar{\rho}}\varepsilon_{\rho}] = \frac{1}{\alpha-\alpha\beta_1+\beta_1}\sigma_\rho^2 \tag{c.7}$$

The standard deviation of the smoothed code measurement at steady state can be expressed as:

$$\begin{aligned}&E[\varepsilon_{\bar{\rho},k}\varepsilon_{\bar{\rho},k}] \\ &= E[(\frac{1}{\alpha}\varepsilon_{\rho,k} + \frac{\alpha-1}{\alpha}(\varepsilon_{\bar{\rho},k-1} + \varepsilon_{\phi,k} - \varepsilon_{\phi,k-1}))^2]\end{aligned}$$

After expanding the above equation and eliminating zero correlation terms, the standard deviation of the smoothed code measurement can be re-written as:

$$\sigma_{\bar{\rho}}^2 = E[\varepsilon_{\bar{\rho},k}\varepsilon_{\bar{\rho},k}]$$
$$= \frac{1}{\alpha^2}E[\varepsilon_{\rho,k}{}^2] + 2\frac{\alpha-1}{\alpha^2}(E[\varepsilon_{\rho,k}\varepsilon_{\bar{\rho},k-1}] + E[\varepsilon_{\bar{\rho},k-1}(\varepsilon_{\phi,k} - \varepsilon_{\phi,k-1})])$$
$$+ (\frac{\alpha-1}{\alpha})^2(E[\varepsilon_{\bar{\rho},k-1}{}^2] + E[(\varepsilon_{\phi,k} - \varepsilon_{\phi,k-1})^2])$$

Substituting $\varepsilon_{\rho,k}$ and $\varepsilon_{\phi,k}$ in the second, third and fifth expectation-function terms using (c.3), and eliminating zero correlation terms yiels:

$$\sigma_{\bar{\rho}}^2 = \frac{1}{\alpha^2}\sigma_{\rho}^2 + (\frac{\alpha-1}{\alpha})^2\sigma_{\bar{\rho}}^2 + 2\frac{\alpha-1}{\alpha^2}\beta_1 E[\varepsilon_{\rho,k-1}\varepsilon_{\bar{\rho},k-1}]$$
$$+ 2(\frac{\alpha-1}{\alpha})^2(\beta_2 - 1)E[\varepsilon_{\bar{\rho},k-1}\varepsilon_{\phi,k-1}] + 2(\frac{\alpha-1}{\alpha})^2(1-\beta_2)\sigma_{\phi}^2$$

At steady-state, we can replace $E[\varepsilon_{\rho,k-1}\varepsilon_{\bar{\rho},k-1}]$ and $E[\varepsilon_{\bar{\rho},k-1}\varepsilon_{\phi,k-1}]$ using previously derived correlation results in (c.7) and (c.6):

$$\sigma_{\bar{\rho}}^2 = \frac{1}{\alpha^2}\sigma_{\rho}^2 + (\frac{\alpha-1}{\alpha})^2\sigma_{\bar{\rho}}^2 + 2\frac{\alpha-1}{\alpha^2}\beta_1\frac{1}{\alpha-\alpha\beta_1+\beta_1}\sigma_{\rho}^2$$
$$+ 2(\frac{\alpha-1}{\alpha})^2(\beta_2-1)\frac{\alpha-\alpha\beta_2-1+\beta_2}{\alpha-\alpha\beta_2+\beta_2}\sigma_{\phi}^2 + 2(\frac{\alpha-1}{\alpha})^2(1-\beta_2)\sigma_{\phi}^2$$

After re-arranging terms, the result is expressed as:

$$[1-(\frac{\alpha-1}{\alpha})^2]\sigma_{\bar{\rho}}^2 = (\frac{1}{\alpha^2} + 2\frac{\alpha-1}{\alpha^2}\frac{\beta_1}{\alpha-\alpha\beta_1+\beta_1})\sigma_{\rho}^2$$
$$+ [2(\frac{\alpha-1}{\alpha})^2(\beta_2-1)\frac{\alpha-\alpha\beta_2-1+\beta_2}{\alpha-\alpha\beta_2+\beta_2} + 2(\frac{\alpha-1}{\alpha})^2(1-\beta_2)]\sigma_{\phi}^2$$
$$\Rightarrow \frac{2\alpha-1}{\alpha^2}\sigma_{\bar{\rho}}^2 = (1 + \frac{2(\alpha-1)\beta_1}{\alpha-\alpha\beta_1+\beta_1})\frac{\sigma_{\rho}^2}{\alpha^2} + 2\frac{(\alpha-1)^2(1-\beta_2)}{\alpha-\alpha\beta_2+\beta_2}\frac{\sigma_{\phi}^2}{\alpha^2}$$

$$\sigma_{\bar{\rho}}^2 = \frac{\alpha+\alpha\beta_1-\beta_1}{(2\alpha-1)(\alpha-\alpha\beta_1+\beta_1)}\sigma_{\rho}^2 + \frac{2(\alpha-1)^2(1-\beta_2)}{(2\alpha-1)(\alpha-\alpha\beta_2+\beta_2)}\sigma_{\phi}^2 \quad \text{(c.8)}$$

For the example used in sections IV and V, which assumes that raw code and carrier multipath errors are uncorrelated in time, we have β_1=0 and β_2=0. Numerical simulations show that two-times smoothing time is needed to achieve steady state and the correlation time constant for the smoothed code is equal to the smoothing time. Therefore, a steady-state 100-second smoothed code measurement actually contains previous measurement information from up to 200 seconds in the past (i.e., beyond the 100 second smoothing time). Therefore, a 30-minute long batch interval using 100-second smoothed code measurements actually exploits information from measurement processed over a '30 minutes plus 200 seconds'. The resulting 2000 second interval is equivalent to the time needed to reach steady state for a 1000-second smoothed code measurement.

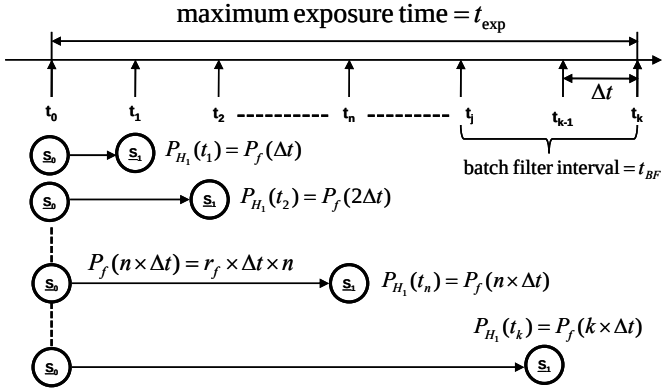

Figure d.1. Satellite health state transition during one hour prior to the current time

Appendix D

A batch estimator exploits GPS measurements collected over multiple epochs. Therefore, the probability of having faulty measurements is different from that of a snap-shot positioning process, which only uses measurements at one epoch in time. Under the single-satellite failure assumption, the prior probability of having one or more faulty measurements within a batch is a function of the batch interval length and the number of measurements within the batch interval.

No more than one satellite failure is assumed during an aircraft approach. The satellite failure rate is r_f = 1x10^{-5} /hr/per SV. An average delay-to-inform-users period t_{exp} of 1 hour is considered. All possible satellite failure scenarios are displayed in Fig. d.1.

In Fig. d.1, s_0 represents a satellite in a healthy status and s_1 represents a satellite failure. The current time tag is t_k and the starting time tag is t_0. The satellite is exposed to a fixed failure rate between t_0 and t_k. The period t_k minus t_0 is equal to1 hr. Every time tag in Fig. d.1 is equally spaced by a sampling interval Δt. The initial satellite status is healthy at time t_0 with a probability of one, because we assumed an external integrity monitoring system that detects any satellite failure happening one hour before t_k and informs the user. The probability of a satellite being in a failure state at epoch n is equal to $P_f = r_f \times \Delta t \times n$. Therefore, the probability that the measurement at epoch n is faulty is $P_{H_1}(t_n) = P_f(n\times\Delta t)$. Assuming that we collect all measurements at each epoch over one hour, the measurement vector is:

$$\vec{m}_{1hr} = \begin{bmatrix} m_0 & m_1 & m_2 & \cdots & m_k \end{bmatrix}^T$$

We are considering the probability of an event n that has faulty measurements starting from epoch n or measurement m_n. We also conservatively assume that the measurements after m_n have a probability of one to be faulty. Therefore, the probability of event n is computed as:

$$P(\text{event } n) = [\prod_{m=1}^{n-1}(1 - P_{H_1}(t_m))P_{H_1}(t_n)] \times 1^{(k-n)}$$
$$= \prod_{m=1}^{n-1}(1 - P_{H_1}(t_m))P_{H_1}(t_n)$$

When the batch interval t_{BF} is smaller than one hour, the measurements included in the batch are from m_j to m_k. The prior probability of one or more faulty measurements in the batch is the sum of event probabilities from event j to k:

$$P_{H_1} = \sum_{n=j}^{k} P(\text{event } n)$$
$$= \sum_{n=j}^{k} \prod_{m=1}^{n-1}(1 - P_{H_1}(t_m))P_{H_1}(t_n)$$